

1 Determining the Plio-Quaternary uplift of the southern French massif-Central; a new insights
2 for intraplate orogen dynamics.

3

4 Oswald Malcles¹, Philippe Vernant¹, Jean Chéry¹, Pierre Camps¹, Gaël Cazes^{2,3}, Jean-François
5 Ritz¹, David Fink³.

6 ¹Geosciences Montpellier, CNRS-University of Montpellier, Montpellier, France

7 ²SEES, University of Wollongong, Wollongong, Australia

8 ³Australian Nuclear Science and Technology Organisation, Lucas Heights, Australia

9

10 *Correspondence to:* Oswald Malcles (oswald.malcles@umontpellier.fr)

11 **Abstract.**

12 The evolution of intra-plate orogens is still poorly understood. Yet, this is of major importance for
13 understanding the Earth and plate dynamic, as well as the link between surface and deep geodynamic
14 processes. The French Massif Central is an intraplate orogen with a mean elevation of 1000m, with
15 the highest peak elevations ranging from 1500m to 1885m. However, active deformation of the region
16 is still debated due to scarce evidence either from geomorphological or geophysical (i.e. geodesy and
17 seismology) data. Because the Cévennes margin allows the use of karst sediments geochronology and
18 morphometrical analysis, we study the vertical displacements of that region: the southern part of the
19 French Massif-Central. Geochronology and morphometrical results, helped with lithospheric-scale
20 numerical modelling, allow, then, a better understanding of this intraplate-orogen evolution and
21 dynamic.

22 Using the ability of the karst to durably record morphological evolution, we first quantify the
23 incision rates. We then investigate tilting of geomorphological benchmarks by means of a high-
24 resolution DEM. We finally use the newly quantified incision rates to constrain numerical models and
25 compare the results with the geomorphometric study.

26 We show that absolute burial age (¹⁰Be/²⁶Al on quartz cobbles) and the paleomagnetic analysis of
27 karstic clay deposits for multiple cave system over a large elevation range correlate consistently. This
28 correlation indicates a regional incision rate of 83^{+17}_{-5} m.Ma⁻¹ during the last ca 4 Myrs (Plio-
29 Quaternary). Moreover, we point out through the analysis of 55 morphological benchmarks that the
30 studied region has undergone a regional southward tilting. This tilting is expected as being due to a
31 differential vertical motion between the north and southern part of the studied area.

32 Numerical models show that erosion-induced isostatic rebound can explain up to two-thirds of the
33 regional uplift deduced from dating technics and are consistent with the southward tilting obtain from
34 morphological analysis. We presume that the remaining part is related to dynamic topography or
35 thermal isostasy due to the Massif Central plio-quaternary magmatism.

36 **1 Introduction and Tectonic Setting**

37 1.1 Introduction

38 Since the past few decades, plate-boundary dynamics is to a first order, well understood. Such is not
39 the case for intraplate regions, where short-term (10^3 - 10^5 yrs.) strain rates are low and the underlying
40 dynamical processes are still in debate (e.g. Calais et al., 2010; Vernant et al., 2013; Calais et al.,
41 2016; Tarayoun et al., 2017). On geological time-scales, transient phenomenon that are classically
42 used to explain intraplate deformations (as seen through the seismic activity) can not be a satisfactory
43 explanation though, this then raises the question of the origin of the high finite deformations observed
44 in many parts of the world as for instance the Ural mountains in Russia, the Blue Mountains in
45 Australia or the French Massif Central.

46 In this study we focus on the Cevennes Mountains and the Grands Causses regions that form the
47 southern part of the French Massif Central, located in the southwestern Eurasian plate (fig.1). The
48 region is characterized by a mean elevation of 1000 m with summits higher than 1500 m. Such
49 topography is likely to be the result of recent, active uplift and as the Cevennes mountains experiences
50 an exceptionally high mean annual rainfall (the highest peak, Mount Aigoual, records the highest
51 mean annual rainfall in France of 4015 mm) it raises the question of a possible link between erosion
52 and uplift as previously proposed for the Alps (Champagnac et al., 2007; Vernant et al., 2013;
53 Nocquet et al., 2016). This region currently undergoes a small but discernible deformation, but no
54 significant quantification can be deduced due to the scarcity in seismicity (Manchuel et al., 2018). In
55 addition, GPS velocities are below the uncertainty threshold of GPS analyses (Nocquet et Calais,
56 2003; Nguyen et al., 2016).

57 South and West of the crystalline Cevennes mountains, prominent limestone plateaus, named Grands
58 Causses, rise to 1000m and are dissected by few canyons that are several hundreds of meter deep (the
59 color-coded-altitude map and the topographic cross-section of figure 1 illustrate the first order
60 topography and morphology of the area). The initiation of incision, its duration and the geomorphic
61 processes leading to the present-day landscape remain poorly constrained. A better understanding of
62 the processes responsible for this singular landscape would bring valuable information on intraplate
63 dynamics, especially where large relief exists.

64

65 The oldest formations in the area were formed during the Variscan orogeny (late Palaeozoic, ~300
66 Ma; Bricchau et al., 2007) and constitute the crystalline basement of the Cevennes. Between 200 and
67 40 Ma (Mesozoic and lower Cenozoic), the region was mainly covered by the sea ensuring the
68 development of an important detrital and carbonate sedimentary cover, which can reach several km
69 thick in some locations (Sanchis and Séranne, 2000; Barbarand et al., 2001). During the Mesozoic era,
70 an episode of regional uplift and subsequent erosion and alteration (called the Durancian event) is
71 proposed as being at the origin of the flat, highly elevated surface that persists today across the
72 landscape (Bruxelles, 2001; Husson, 2014).

73 The area is also affected by the major NE-SW trending Cevennes fault system. During the Pyrenean
74 orogeny, 85 to 25 Ma (Tricart, 1984; Sibuet et al., 2004), several faults and folds affected the
75 geological formations south of the Cevennes fault, while very few deformations occurred further

79 north within the Cévennes and Grand Causses areas (Arthaud and Laurent, 1995). Eventually, the
80 Oligocene extension (~30 Ma) led to the counterclockwise rotation of the Corso-Sardinian block and
81 the opening of the Gulf of Lion, re-activating some of the older compressive structures as normal
82 faults. The main drainage divide between the Atlantic Ocean and the Mediterranean Sea is located in
83 our study area and is inherited from this extensional episode (Séranne et al., 1995; Sanchis et al.,
84 2000).

85 Superimposed at the inheritance from Durancian event, the last two major tectonic episodes which are
86 the Pyrenean compression and the Oligocene extension shaped the large-scale structural morphology
87 of the region. Afterwards during the Plio-Quaternary period, only intense volcanic activity has
88 affected the region, from the Massif Central to the Mediterranean shoreline. This activity is
89 characterised by several volcanic events that are well constrained in age (Dautria et al., 2010). The
90 last eruption occurred in the Chaîne des Puys during the Holocene (i.e. the past 10 kyrs (Nehlig et al.,
91 2003; Miallier et al., 2004). Some authors proposed that this activity is related to a hotspot underneath
92 the Massif Central (Granet et al., 1995; Baruol and Granet, 2002) leading to an observed positive
93 heat-flow anomaly and a possible regional plio-Quaternary uplift.

94 Despite this well described overall geological evolution the onset of active incision that has
95 shaped the deep valleys and canyons (e. g. Tarn or Vis river, Fig 1) across the plateaus, and the
96 mechanisms that controlled this incision are still in debate. One hypothesis proposes that canyon
97 formation was driven by the Messinian salinity crisis with a drop of more than 1000m in
98 Mediterranean Sea level. This, however, would then not explain the fact that the Atlantic watersheds
99 show similar incision. Other studies suggested that the incision is controlled by the collapse of cave
100 galleries that lead to fast canyon formation mostly during the late Quaternary, thus placing the onset
101 of canyon formation only a few hundreds of thousands of years ago (Corbel, 1954). In contrast, it has
102 also been proposed more recently (based on relative dating techniques and sedimentary evidence) that
103 incision during the Quaternary was negligible (i.e. less than a few tens of meters), and that the
104 regional morphological structures seen today occurred around 10 Ma (Séranne et al., 2002; Camus,
105 2003).

106

107 1.2 Working hypothesis

108 In this paper, we provide new quantitative constraints on both the timing of incision and the
109 rate of river down-cutting in the central part of the Cévennes and of the Grands Causses that has
110 resulted in the large relief between plateau and channel bed. We employ two methods, cosmogenic
111 $^{10}\text{Be}/^{26}\text{Al}$ burial dating quartz cobbles that have been transported by rivers and paleomagnetic analyses
112 along vertical profiles of endokarstic clay both of which have been deposited in multiple cave systems
113 at the time cave entry was at river channel elevation. In parallel, by analysing a high-resolution DEM
114 (5m), we show that the region is affected by a regional tilting. Our results allow to quantify the role of
115 the Plio-Quaternary incision on the Cévennes landscape evolution and to constrain numerical
116 modelling from which we derive the regional uplift rates and a tilt of geomorphological markers.

117

118 One important point of this study is the integration of multi-disciplinary approaches in order
119 to constrain intraplate deformation. Such an approach is necessary to bring new insights into the
120 lithosphere behaviour of slow dynamic regions. If the uplift is easily recognisable in the landscape
121 (1000 m high plateaus), quantifying its timing and evolution rates is harder and can't be performed by
122 classical technics (e.g. GPS). This is why we aim to quantify the incision rate over the longest
123 possible period thanks to the karstic immunity. Dealing with long-term incision rates (up to 5 Myrs)
124 should permit to smooth possible climatic-driven incision rate variations (with time-span of several
125 kyrs).

126 If incision is initiated by uplift centred on the North of the area where elevations are maximum, it will
127 lead to tilting of fossilised topographic markers as strath terraces. Our method of analyses provides
128 an opportunity to select between three possible explanations for the current terrain morphology. The
129 first is based on old uplift and old incision (Fig. 2.A). In this case, apparent incision rates would be
130 very low. For instance, if incision commenced 10 Ma (Serrane et al., 2002), we would find surface
131 tilting but cosmogenic burial dating with $^{10}\text{Be}/^{26}\text{Al}$ which cannot discern ages older than $\sim 5\text{Ma}$ due to
132 excessive decay of ^{26}Al , would not be possible. The second possibility (Fig. 2.B) is that the uplift is
133 old, and incision consequently follows but with a time lag. Here the incision rate would be rather fast
134 but no tilting is expected for the river-related markers because no differential uplift occurs after their
135 formation. Finally, the third possibility (Fig 2.C) is that uplift and incision are concurrent and recent
136 (i.e. within the time scale of cosmogenic burial dating) and thus we would expect burial ages < 5
137 Myrs relatively high incision rates, and tilting of morphological markers. These different proposals
138 for the temporal evolution of the region will then be compared using numerical modelling.

139

140

141 **2. Determining the incision rates in the Cévennes and the Grand Causses Region**

142 **2.1. Principles and methods**

143 **2.1.1. Karst model**

144 No evidence of important aggradation events has been reported in the literature for the studied area.
145 Therefore we base our analysis on a per descensum infill model of the karst networks whereby
146 sediments are transported and then deposited within cave galleries close to base level. When cave-
147 systems and entry passages are near the contemporaneous river channel elevation (including higher
148 levels during floods), the deposition into caves of sediments, from clay to cobbles occurs, especially
149 during flood events. Subsequent river incision into bedrock creates a relative base level drop (due to
150 uplift or sea-level variations). The galleries associated with the former base-level are now elevated
151 above the new river course and become disconnected from further deposition. Hence fossilised and
152 trapped sediments throughout the cave network represent the cumulative result of incision. In this

153 commonly used model (Granger et al., 1997; Audra et al., 2001; Stock et al., 2005; Harmand et al.,
154 2017), the higher the gallery elevation (relative to the present-day base level) the older the deposits in
155 that gallery. As a result, the objective here is to quantify a relative lowering of the base level in the
156 karst systems, with the sediments closest to the base level being the youngest deposits, and note that
157 we do not date the cave network creation which may very well pre-date river sediment deposition.
158 Within individual canyons, successions of gallery networks across the full elevation range from
159 plateau top to modern river channel, were not always present and often sampling could not be
160 conducted in a single vertical transect. Thus we make the assumption of lateral altitudinal continuity
161 i.e. that within a watershed, which may contain a number of canyons, the sediments found in galleries
162 at the same elevation were deposited at the same time. Inside one gallery, we use the classical
163 principle of stratigraphy sequence (i.e. the older deposits are below the younger ones). More details
164 on the karst network geometry and its relation to morphological markers can be find in Camus (2003).
165 Dating accurately the emplacement of cave galleries is a challenge and beyond the scope of this paper.
166 We only aim at using the dating information brought by sediment that have been trapped into the cave
167 system. Therefore, we apply the classical model (e.g. Harmand et al., 2017) where sediments in cave
168 opened on canyon walls are related to terraces or other geomorphologic markers. In this kind of
169 context, former studies suggest that the hypotheisis is valuable (i.e. Granger et al., 1997, 2001). For
170 cave topographic surveys, we refer the reader to the Karst3D database (Karst3D, 2019).

171 **2.1.2. Burial ages**

172 Burial dating using Terrestrial cosmogenic nuclides (TCN) is nowadays a common tool to quantify
173 incision rates in karstic environment (Granger and Muzikar, 2001; Stock et al., 2005; Moccochain.,
174 2007; Tassy et al., 2013; Granger et al., 2015; Calvet et al., 2015; Genti, 2015; Olivetti et al., 2016;
175 Harmand et al., 2017; Rovey II et al., 2017; Rolland et al., 2017; Sartégou, 2017; Sartégou et al.,
176 2018). This method relies on the differential decay of TCN in detrital rocks that were previously
177 exposed to cosmic radiation before being trapped in the cave system. With this in mind, the ^{10}Be and
178 ^{26}Al nuclide pair is classically used as (i) both nuclides are produced in the same mineral (i.e. quartz),
179 (ii) their relative production ratio is relatively well constrained (we use here a standard $^{26}\text{Al}/^{10}\text{Be}$ pre-
180 burial ratio of 6.75, see Balco et al., 2008) and (iii) their respective half-lives (about 1.39 Myr and
181 0.70 Myr for ^{10}Be and ^{26}Al , respectively) are well suited to karstic and landscape evolution study, with
182 a useful time range of ~ 100 ky to ~ 5 Myr.

183 To quantify the incision rate of the limestone plateau of the Cevennes area, we analysed quartz
184 cobbles infilling from four caves of the Rieutord canyon (Fig. 1), this canyon is well suited for such
185 study because horizontal cave levels are tiers over 200 m above the current river-level and are directly
186 connected to the canyon, leading to a straight relationship between river elevation and the four cave
187 infilling that we have sampled (Cuillère cave, Route cave, Camp-de-Guerre cave and Dugou cave).
188 Furthermore, cobbles source is well known and identified: the upstream part of the Rieutord river,
189 some tens of kilometers northward, providing a unique sediment origin composed of granite and

190 metamorphic rocks embedding numerous quartz veins.. All samples (Example Fig. 3) were collected
191 far enough away (>20m) from the cave entrance and deep enough below the surface (>30m) to avoid
192 secondary in-situ cosmogenic production of ^{10}Be and ^{26}Al in the buried sediments.

193

194 The quartz cobbles were first crushed and purified for their quartz fraction by means of sequential
195 acid attack with Aqua-Regia ($\text{HNO}_3 + 3\text{HCl}$) and diluted Hydrofluoric acid (HF). Samples were then
196 prepared according to ANSTO's protocol (see Child et al. 2000) and $\sim 300\mu\text{g}$ of a ^9Be carrier solution
197 was added to the purified quartz powder before total dissolution. AMS measurements were performed
198 on the 6MV SIRIUS AMS instrument at ANSTO and results were normalised to KN-5-2 (for Be, see
199 Nishiizumi et al., 2007) and KN-4-2 (for Al) standards. Uncertainties for the final ^{10}Be and ^{26}Al
200 concentrations include AMS statistics, 2% (Be) and 3% (Al) standard reproducibility, 1% uncertainty
201 in the Be carrier solution concentration and 4% uncertainty in the natural Al measurement made by
202 ICP-OES, in quadrature. Sample-specific details and results are found in table 1.

203

204 **2.1.3. Paleomagnetic analysis**

205 In parallel with burial dating, we analyzed the paleomagnetic polarities of endokarstic clay
206 deposits within two main cave systems: the *Grotte-Exurgence du Garrel* and the *Aven de la Leicasse*
207 (Fig. 1). These two cave systems allowed us collecting samples along a more continuous range of
208 elevations than the one provided by the Rieutord samples (for burial age determination) and also
209 extending the spatial coverage to the Southern Grands Causses region. Thanks to the geometry of
210 these two cave systems, we sampled a 400m downward base level variation. The sampling was done
211 along vertical profiles from a few ten of centimeters to 2 meters high by means of Plexiglas cubes
212 with a 2 cm edge length (Fig. 4) used as a pastry cutter. We weren't able to analyse clay samples from
213 Rieutord canyon because no reliable clay infilling was found in the Rieutord caves.

214 Demagnetisation was performed with an applied alternative field up to 150mT using a 2G-760
215 cryogenic magnetometer, equipped with the 2G-600 degausser system controller. Before this analysis,
216 each sample remained at least 48h in a null magnetic field, preventing a possible low coercivity
217 viscosity overprinting the detrital remanent magnetisation (DRM) (Hill, 1999; Stock et al., 2005;
218 Hajna et al., 2010). If the hypothesis of instantaneous locked in DRM seems reasonable compared
219 with the studied time span, it is important to keep in mind that the details of DRM processes (as for
220 instance the locked in time) is not well understood (Tauxe et al., 2006; Spassov et Valet, 2012) and
221 could possibly lead to small variations (few percents) in the following computed incision rates.

222 Because fine clay particles are expected being easily reworked in the cave, careful attention was paid
223 to the site selection and current active galleries were avoided. Clays deposits had to show well
224 laminated and horizontal layering in order to prevent analysis of in-situ produced clays (from
225 decalcification) or downward drainage by an underneath diversion gallery that could strongly affect

226 the obtained inclination (and also the declination to a minor extent). Note that for paleo-polarities
227 study alone, small inclination or declination variations won't result in false polarities

228 **2.2 Quantifying the average incision rates**

229 **2.2.1. Rieutord incision rate from burial ages**

230

231 The relationship between burial ages and incision is shown in Figure 5. For the four caves, we
232 observed a good correlation between burial ages and finite incision, except for the Camp-de-Guerre
233 cave (CDG) site, the higher the cave is, the older the burial ages are. Burial ages for the Cuillère cave,
234 Dugou cave, Camp-de-Guerre cave and Route cave are 2.16 ± 0.15 , 0.95 ± 0.14 , 0.63 ± 0.1 and $0.21 \pm$
235 0.1 Myrs respectively. This is consistent with the supposed cave evolution and first-order constant
236 incision of the Rieutord canyon. CDG age has to be considered with caution. The CDG cave entrance
237 located in a usually dry thalweg can act as a sinkhole or an overflowing spring depending on the
238 intensity of the rainfall. The sample was collected in a gallery showing evidence of active flooding
239 ~10 m above the Rieutord riverbed, therefore the older than expected age, given the elevation of the
240 cave, is probably due to cobbles that came from upper galleries during flood events. Forcing the linear
241 regression to go through the origin, leads to an incision rate of 83 ± 35 m.Ma⁻¹. These results show
242 that at least half of the 300 m deep Rieutord Canyon is a Quaternary incision. Extrapolating the
243 obtained rate yields an age of 4.4 ± 1.9 Ma for the beginning of the canyon incision, which suggests
244 that the current landscape has been shaped during the Plio-Quaternary period. To extend our spatial
245 coverage and bring stronger confidence into our results, we combine Rieutord burial ages with
246 paleomagnetic data from watersheds located on the other side of the Herault watershed.

247 **2.2.2. South Grands Causses incision rate from paleomagnetic data**

248 A total of 141 clay-infilling samples distributed over 13 profiles in 2 caves were studied. The lowest
249 sample elevation above sea level (a.s.l.) is in the Garrel (ca 190 m) and the highest is in the Leicasse
250 (ca 580 m a.s.l.). In the Leicasse cave system, we sampled 8 profiles totalizing 61 samples. Profiles
251 elevations are located between ca 200 m and ca 400 m above the base level (a.b.l.), which corresponds
252 to the elevation of the Buèges river spring at 170 m a.s.l.

253 In the Garrel cave system, we sampled 5 profiles totalizing 80 samples that range between 20 m and
254 80 m a.b.l. defined by the Garrel spring at 180 m a.s.l. Given the very marginal difference in elevation
255 between the local base levels from these two caves, we assume that they have the same local base
256 level. At each studied site, if all the profile samples have the same polarity, the site is granted with the
257 same polarity, either normal or reverse. If not (i.e. the profile displays normal and reverse polarities),
258 we consider it as a transitional site. Figure 6 shows the results plotted with respect to the
259 paleomagnetic scale (x axis) for the past 7 Ma, and their elevation above the base level (y axis). The
260 measured paleomagnetic polarities on each sites are plotted for several given incision rates supposed
261 to be constant through times (this allows determining different incision rate models and analyze their

262 correlation with the distribution of paleomagnetic data, see below). First, we note a good agreement
263 between samples located at the same elevation and being part of the same stratigraphic layer (Camus,
264 2003). This syngenetic deposition allow, as best explanation to prevent from a possible partial
265 endokarstic reworking. Second, the different elevations of the galleries where we collected the
266 samples allow proposing that the Leicasse deposits encompass at least three chrons, while the Garrel
267 deposits encompass only one. Third, a transitional signal comprised between a reversal signal (lower
268 samples) and a normal signal (upper ones) is observed at Les Gours sur Pattes (LGP, Leicasse cave)
269 sampling site (Fig. 7). This provides a strong constraint on the age of the sediment emplacement in the
270 Leicasse with respect to the magnetostratigraphic timescale (Fig. 6).

271 Compared to the Leicasse cave system, the elevation/polarity results for the Garrel are less
272 constrained. Only one site shows a reverse polarity at 90 m a.b.l., and the transitional polarity found at
273 40 m a.b.l. is unclear (tab, suppl mat.). The rest of the polarities (72 samples) are all normal. Given
274 that a U-Th ages younger than 90 kyrs was obtained for two speleothems (Camus, 2003) covering our
275 samples collected at 40 m a.b.l. (Fig. 6), we consider that the emplacement of the clays deposits
276 occurred during the most recent normal period and are therefore younger than 0.78 Ma (Figure 6).
277 The transition between the highest normal sample and the reversed one is located somewhere between
278 78 m and 93 m a.b.l. suggesting a maximum base level lowering rate of $109 \pm 9 \text{ m.Ma}^{-1}$.

279 To go further in the interpretation of our data, and better constraint the incision rate, we performed a
280 correlation analysis between observed and modelled polarities for a 0 - 200 m.Ma-1 incision-rate
281 range (linear rate, each 1m.Ma-1). Modelled polarities are found using the intersection between
282 sample elevation and incision-rate line.

283 We obtained 10 possible incision rates with the same best correlation factor (Fig. 8) spanning from 43
284 to 111 m.Ma⁻¹ (mean of $87 \pm 24 \text{ m.Ma}^{-1}$). Taking into account the transitional signal of the LGP site in
285 the Leicasse cave yields a linear incision rate of $83^{+17}_{-5} \text{ m.Ma}^{-1}$. Proposed uncertainties are based on
286 previous and next transition-related estimated incision rate.

287 Using a similar approach for the Rieutord crystalline samples where we minimize the residual
288 between the observed and the modeled ages based on the same incision-rate range than for the
289 paleomagnetic samples. With this method, we determined a linear incision rate of $85 \pm 11 \text{ m.Ma}^{-1}$ (Fig
290 8). Those two results, based on independent computations, suggest the same first-order incision rate
291 for the last 4 Ma of $84^{+21}_{-12} \text{ m.Ma}^{-1}$. Given that the Rieutord, Garrel and Buèges rivers are all
292 tributaries of the Hérault river, we propose that this rate represents the incision rate for the Hérault
293 river watershed, inducing approximately 300-350 m of finite incision over the Plio-Quaternary period.
294 If the landscape is at first order in an equilibrium state, that is to say, if we preclude our incision rates
295 being a regressive erosional signal, the incision needs to be balanced by an equivalent amount of
296 uplift. If the uplift rate is roughly correlated to the regional topography, lowest uplift rates would be
297 expected in the south of our sampling sites inducing regional tilting of morphological benchmarks. In
298 the next part, we search for such evidences that would suggest differential uplift.

299

300 2.3 Geomorphometrical approach

301 According to the Massif-Central centered uplift hypothesis, morphological markers such as strath
302 terraces, fluvio-karstic surfaces or abandoned meanders should display a southward tilting due to
303 differential uplift between the northern and the southern part of the region.

304 To investigate these different signals, we used the morphological markers available for the
305 study area (Fig. 9). We used a 5 m resolution DEM analysis to identify the markers corresponding to
306 surfaces with slope $< 2^\circ$. This cut-off slope angle prevents to identify surface related to local
307 deformation such as for example landslide or sinkhole. Diffusion processes could create apparent tilt
308 of remnant horizontal surfaces. However, we avoid that problem by completing the automatic
309 selection and correction with a final check to make sure that the residuals are randomly distributed
310 over the surface (see below). The local river slope is on the order of 0.1° so the 2° cut-off angle is far
311 from precluding to identify tilted markers. We also use a criterion based on an altitudinal range for a
312 surface. This altitudinal span is set individually for each surface based on elevation, slope and curves
313 map analysis, and encompass from few meters to tens of meters depending on the size of the marker.
314 We checked 80% of the identified surfaces in the field in order to avoid misinterpretation. Some
315 pictures are provided in supplementary material. The dip direction and angle of the surface in
316 computed in a two steps approach. First, we fit a plan using extracted points from the DEM inside the
317 delimited surface. Second, based on this plan we remove the DEM points with residuals 3 times larger
318 than the standard error and compute more accurate plan parameters (second fitting). This outlier
319 suppression removes any inaccurate DEM points and correct for inaccurate surface delimitation (e.g.
320 integration of a part of the edge of a strath terrace, diffusion processes marks, etc.).

321 Because no obvious initially horizontal markers are known, we propose to correct the marker current
322 slope by the initial one to quantify the tilt since the marker emplacement. To do so we follow the
323 method used by Champagnac et al. (2008) for the Forealps. We identify the drain related to the marker
324 formation and compute its current local slope and direction. This method assumes that landscapes are
325 at the equilibrium state and that the river slope remained constant since the marker formation. This
326 assumption seems reasonable given the major river profiles and because most of the markers used are
327 far from the watershed high altitude areas precluding a recessive erosional signal. Finally, we
328 removed the local river plan from the DEM extracted surface.

329 Following this methodology, we obtained 61 surfaces. We then applied three quality criterions to
330 ensure the robustness of our results: 1) The minimal surface considered is 2500 m^2 based on a
331 comparison between the 5m resolution DEM and a RTK GPS survey over 3 strath terraces (Hérault
332 river); 2) Final plans with dip angles larger than 2° are removed; 3) The residuals for each
333 geomorphological marker must be randomly distributed without marker edge signal, or clear
334 secondary structuration. Only 38 markers meet those 3 quality criterions.

335 If the identified and corrected markers have indeed registered a differential uplift between the north
336 and the south, we expected the following observations:

337 - The dipping direction of the tilted markers should be parallel to the main gradient of the topography,
338 i.e. between 150°E and 180°E for our studied region. This expectation is the most important one,
339 regarding uncertainties on the uplift rate and lithospheric elastic parameters.

340 - A latitudinal tilting trend, i.e. an increase of the tilt angle along the topography gradient. Indeed, null
341 or small tilts are expected near the shoreline and within the maximum uplift area of the
342 Cevennes/Massif Central, while the maximum tilt is expected at a mid-distance between these two
343 regions, i.e. about 50 km inland from the shoreline.

344 - A positive altitudinal tilting trend (an increase in dip angle with altitude). This trend would be
345 representative of the accumulation of finite tilt. However, it supposes a linear relationship between the
346 altitude and the age of the marker formation. If at first order, this straightforward hypothesis seems
347 reasonable for river-controlled markers (e.g. strath terraces), other surfaces are hardly expected to
348 follow such an easy correlation.

349

350 Only the southward dip seems to be robust with a mean tilt angle of $0.60 \pm 0.40^\circ$ with an azimuth of
351 $N128 \pm 36^\circ E$ (Fig. 10). Latitudinal and altitudinal trends are less robust but that is not surprising
352 because of the strong susceptibility to local phenomenon and the lack of robust age constrains.

353

354 **3 Numerical modelling**

355 Both geomorphological and geochronological evidence suggest a Plio-Quaternary uplift of the
356 Cevennes area. The origin of such uplift could be associated with several processes: erosion-induced
357 isostatic rebound, dynamic topography due to mantle convection, thermal isostasy, residual flexural
358 response due to the Gulf of Lion formation, etc. For the Alps and Pyrenees mountains, isostatic
359 adjustment due to erosion and glacial unloading has been recently quantified (Champagnac et al.,
360 2007, Vernant et al., 2013; Genti et al, 2016, Chery et al. 2016). Because the erosion rates measured in
361 the Cevennes are similar to those of the Eastern Pyrenees (Calvet et al., 2015, Sartégou et al., 2018a),
362 we investigate by numerical modelling how an erosion-induced isostatic rebound could impact the
363 southern Massif Central morphology and deformation.

364 We define a representative cross-section parallel to the main topographic gradient (i.e. NNW-SSE)
365 and close to the field investigation areas (Figure 11). We study the lithospheric elastic response to
366 erosion with the 2D finite element model ADELI (Hassani et Chery, 1996; Chéry et al. 2016). The
367 model is composed of a plate accounting for the elasticity of both crust and uppermost mantle.
368 Although the lithosphere rigidity of the European plate in southern Massif central is not precisely
369 known, vertical gradient temperatures provided by borehole measurements are consistent with heat
370 flow values ranging from 60 to 70 mW.m² (Lucazeau et Vasseur, 1989). Therefore, we investigate
371 plate thickness ranging from 10 to 50 km as done by Stewart et Watts (1997) for studying the vertical
372 motion of the alpine forelands. We choose values for Young's and Poisson parameters of respectively

373 10^{11} Pa and 0.25, both commonly used values for lithospheric modelling (e.g. Kooi et Cloething,
374 1992; Champagnac et al. 2007, Chéry et al., 2001). This leads to long-term rigidity of the lithosphere
375 model ranging from 10^{21} to 10^{25} N.m. Since the effect of mantle viscosity on elastic rebound is
376 assumed to be negligible at the time scale of our models (1 to 2 Myrs), we neglect the visco-elastic
377 behaviour of the mantle. Therefore, the base of the model is supported by an hydrostatic pressure
378 boundary condition balancing the weight of the lithosphere (Fig. 11). Horizontal displacements on
379 vertical sides are set to zero since geodetic measurements show no significant displacements (Nocquet
380 et Calais, 2003; Nguyen et al., 2016). The main parameters controlling our model are the erosion (or
381 sedimentation) triggering isostatic rebound and the elastic thickness. The erosion profile (Fig. 11) is
382 based on topography, our newly proposed incision rate and other studies (Olivetti et al., 2016 for
383 onshore denudation and Lofi et al., 2003; Leroux et al., 2014 for offshore sedimentation). This profile
384 is a simplification of the one that can be expected from Olivetti et al. (2016) and do not aim at
385 matching precisely the published data because of, first, the explored time-span (~ 1 Myrs) is not
386 covered by thermochronological data (> 10 Myrs) or cosmogenic denudation rate (10s-100s kyrs).
387 Second, we assume that erosion rates are correlated to the first order to the local (10 s km^2) slopes, that
388 are higher near the drainage divide. This allows to include any kind of erosion processes (e.g.
389 landslides). Third, the model supposes a cylindrical structure perpendicular to the cross section, this
390 implies to average the high-frequency lateral variations of slope, elevation, etc. to derive the actual
391 denudation rate based on these proxies. Concerning this erosion profile, a parametric study with
392 highest erosion rate ranging from 1 to 1000 m.Myr^{-1} led to the same first order interpretations.

393 The flexural rigidity controls the intensity and wavelength of the flexural response and ranges
394 from 10^{21} to 10^{25} N.m. It can be expressed as a variation in elastic thickness (T_e) ranging from 4.4 to
395 96 km (Fig. 12). We also test a possible T_e variation between inland and offshore areas. For the
396 following discussion, we use an elastic thickness of 15km corresponding to a value of D of 3.75×10^{23}
397 N.m^{-1} . In this case, the inland and offshore parts are largely decoupled and the large sedimentation rate
398 in the Gulf of Lion does not induce a flexural response on the Cévennes and Grands Causses areas.
399 With a maximum erosion rate of 80 m.Ma^{-1} (Fig 11), the models display uplift rates of 50 m.Ma^{-1} over
400 more than 100 km. As previously explained, the finite incision is permitted by an equal amount of
401 uplift considering that the incision is not due to regressive erosion. If all tested models show uplift,
402 the modelled amplitudes are smaller than the expected ones. To obtain the same uplift rate than the
403 incision rates, the applied erosion rate over the model must be increased. However, we assume that
404 the landscape is at equilibrium, so, if the erosion rate is increased, it will be higher than the incision
405 rate leading to the decay of relief over the area. No evidence of such evolution is found over the
406 region and, if further studies need to be done to quantify the actual erosion rate, we mostly think that a
407 second process is acting, inducing the rest of the uplift that can't be obtained by the erosion-induced
408 isostatic adjustment. Finally, models predict a seaward tilt of the surface at the regional-scale (Fig.
409 13), in agreement with the observed tilting of morphological markers.

410 4. Discussion

411

412 We assume that the sediments collected in the karst were deposited per descensum, i.e. we do
413 not know if the galleries existed a long time before or were formed just before the emplacement of the
414 sediments, but the more elevated the sediments are, the older their deposit is. If there is no evidence of
415 an important aggradation episode leading to more a complex evolution as proposed for the Ardèche
416 canyon (Moccochain et al., 2007; Tassy et al., 2013), we point out that small aggradation or null
417 erosion period could, however, be possible. Some processes could explain such relative stability: e.g.
418 variation in erosion (due to climatic fluctuation) or impact of eustatic variations (in river profile,
419 flexural response, etc.). Such transient variations have been shown for the Alps (Saillard et al., 2014;
420 Rolland et al., 2017) and are proposed as being related to climato-eustatic variations and therefore
421 should last 10 to 100 kyrs at most.

422 Based on our sampling resolution, we cannot evidence such transient periods and we must use an
423 average base level lowering rate in the karst, which we correlate to the incision of the main rivers. The
424 TCN-based incision rate derived from the Rieutord samples ($83 \pm 35 \text{ m.Ma}^{-1}$) is consistent with the
425 one derived from the Garrel (U-Th ages: 85.83 m.Ma^{-1} according to the sole U/Th exploitable result
426 (Camus, 2003)) and from the Garrel-Leicasse combination (Paleomagnetic approach: $84^{+21}_{-12} \text{ m.Ma}^{-1}$).
427 This mean incision rate of ca. 85 m.Ma^{-1} lasting at least 4 Ma, highlights the importance of the Plio-
428 Quaternary period into the Cévennes and Grand Causses morphogenesis. Furthermore, the 300 to 400
429 m of incision precludes a relative base level controlled by a sea-level drop. Indeed, documented sea
430 level variations are less than 100 m (Haq, 1988, Miller et al., 2005). Furthermore, the Herault river
431 does not show any significant knickpoints or evidence of unsteadiness in its profile as expected if the
432 incision was due to eustatic variations. Therefore, we propose that the incision rate of $\sim 85 \text{ m.Ma}^{-1}$ is
433 due to a plio-quaternary uplift of the Cévennes and Grands Causses region.

434

435 Other river-valley processes could lead to a local apparent high incision rate as for instance
436 major landslide or alluvial fan (Ouimet et al., 2008). This hypothesis of an epigenetic formation of the
437 Rieutord is irrelevant because of i) none of the possible causes had been found in the Rieutord canyon
438 and ii) the consistency of the TCN-based incision rate and the paleomagnetic-based incision rate for
439 two other cave-systems. Indeed, the use of two independent approaches and three locations is a good
440 argument in favour of the robustness of our proposed mean 85 m.Ma^{-1} incision rate. Yet, using more
441 data, particularly burial dating colocalized with clays samples and adding sampling sites would give a
442 stronger statistical validation. In the Lodève basin (Point 4, fig. 1), inverted reliefs allow another
443 independent way to quantify minimal incision rate. K/Ar and paleomagnetic dated basaltic flows
444 spanning from 1 to 2 Myrs old that were deposited at the bottom of the former valley (Dautria et al.,
445 2010) are now located at ca 150 m above the current riverbed leading to an average incision rate of 77
446 $\pm 10 \text{ m.Myr}^{-1}$, in agreement with karst-inferred incision rates.

447 Furthermore, preliminary results from canyons on the other side of the Grands Causses (Tarn and

448 Jonte) based on in-situ terrestrial cosmogenic dating suggest similar incision rates (Sartegou et al.,
449 2018b) and confirm a regional base level lowering of the Cévennes and Grands Causses region during
450 the Plio-Quaternary. This is consistent with the similarities of landscapes and lithologies observed
451 both on the Atlantic and Mediterranean watersheds (e.g. Tarn river).

452 Once the regional pattern of the Plio-Quaternary incision established for the Cévennes-Grands
453 Causses area, the next question is how this river downcutting is related to the regional uplift? First
454 order equilibrium shape and absence of major knick points in the main river profiles preclude the
455 hypothesis of regressive erosion. Hence, back to the three conceptual models presented in part 1
456 (Fig.2), we can discard, at first order, the models A (Old uplift-recent incision) and B (Old uplift-old
457 incision) because the obtained incision rate shows recent incision and surface tilting tend to prove a
458 current uplift. Therefore, the incision rate has to be balanced to the first order by the uplift rate.
459 Eustatic variations magnitudes are of too low (100-120 m) to explain the total incision (up to 400m).
460 Furthermore, no obvious evidence of active tectonic is reported for the area raising the question of the
461 processes responsible for this regional uplift. Very few denudation rates are reported for our study
462 area (Schaller et al., 2001; Molliex et al., 2016; Olivetti et al., 2017), and converting canyon incision
463 rates into denudation and erosion rates is not straightforward, especially given the large karst
464 developed in the area. Using a first order erosion/sedimentation profile following the main topography
465 gradient direction we have modelled the erosion-induced isostatic rebound. If this process could
466 create between half and two third of the Plio-Quaternary uplift, a previously existent topography is
467 needed to trigger erosion so it cannot explain neither the onset of the canyon-carving nor the full uplift
468 rates. Other, processes have to be explored such as dynamic topography or thermal anomaly beneath
469 the Massif-Central, the magmatism responsible for the important increase in volcanic activity since ~
470 6 Myrs (Michon et Merle, 2001; Nehlig et al., 2003) could play a major role, notably in the initiation
471 of Plio-Quaternary uplift. Unfortunately, given the age of our samples (0-4 Myrs), discussing the
472 onset of the uplift leading to our observations is out of the scope of this paper.

473

474 **5. Conclusion**

475

476 To the contrary of previous studies that focused on one cave, we have shown that combining
477 karst burial ages and paleomagnetic analysis of clay deposits in several caves over a large elevation
478 range can bring good constraints on incision rates. This multi-cave system approach diminishes the
479 intrinsic limits of the two single methods: low sampling density (and analysis cost) for the TCN ages
480 and difficulty to set the position of paleomagnetic results. Our estimated paleo base level ages are
481 Plio-Quaternary (ca. last 4 Ma) and allow to derive a mean incision rate of 83^{+17}_{-5} m.Ma⁻¹ for the
482 Cevennes area.

483 The landscape, and especially the river profiles suggest a first-order equilibrium allowing
484 considering the incision rate as an uplift rate. We propose that related erosional isostatic adjustment is
485 of major importance for the understanding of the southern French Massif-Central landscape evolution

486 and explain a large part of the uplift. However, it is not the only process involved and we hypothesize
487 that it could be especially combined with dynamic topography related to the Massif Central
488 magmatism. Both mechanisms imply an uplift centered on the Massif Central and a radial tilt of the
489 geomorphological surfaces. We have shown using a geomorphological analysis that at least south of
490 the Cévennes, several surfaces are tilted toward the SSE. This kind of study had been performed
491 before on large structures (Champagnac et al., 2007) or endokarstic markers (Granger et Stock, 2004)
492 but it is the first time that it is performed at such scale with small markers. Numerical modelling
493 yields the same pattern of SSE dipping, allowing more confidence in the geomorphometric results.
494 Our multi-disciplinary approach brings the first absolute dating of the Cévennes landscapes and
495 suggests that the present-day morphology is partly inherited from the plio-quadernary erosion-induced
496 isostatic rebound. A strong uplift impact is assumed to be due to magmatic-related dynamic
497 topography that could explain another part of the uplift as well as the onset of such uplift that has
498 afterward been accelerated by the erosion-induced isostatic rebound. These results enlighten the
499 importance of surface processes into lithospheric-scale dynamic and vertical deformations in intra-
500 plate domains.

501

502 An analysis at the scale of the Massif Central is now needed before nailing down our
503 interpretations, but such study will more likely highlight the importance of erosion processes to
504 explain uplift of intraplate orogens, and will show that another process is needed for the Massif
505 Central, which will most likely be dynamic topography related to magmatism.

506 **References**

507

508 Arthaud F. et Laurent P.: Contraintes, déformations et déplacements dans l'avant-pays pyrénéen du
509 Languedoc méditerranéen, *Godin. Acta*, 8, 142-157, 1995.

510 Audra P., Camus H. et Rochette P.: Le karst des plateaux de la moyenne vallée de l'Ardèche : datation
511 par paléomagnétisme des phases d'évolution plio-quadernaires (aven de la Combe Rajeau). *Bull. Soc.*
512 *Géol. France*, 2001, t. 172. N°1, pp. 121-129, 2001.

513 Balco, G., Stone, J.O., Lifton, N.A., Dunai, T.J., 2008. A complete and easily accessible means of
514 calculating surface exposure ages or erosion rates from Be-10 and Al-26 measurements. *Quat.*
515 *Geochronol.* 3, 174–195. 2008.

516 Barbarand J., Lucazeau F., Pagel M. Et Séranne M.: Burial and exhumation history of the south-
517 eastern Massif Central (France) constrained by en apatite fission-track thermochronology.
518 *Tectonophysics*, 335, 275-290, 2001.

519 Barruol G. et Granet M.: A Tertiary astenospheric flow beneath the southern French Massif Central
520 indicated by upper mantle seismic anisotropy and related to the west Mediterranean extension. *Earth*
521 *and Planetary Science Letters* 202 (2002) 31-47, 2002.

522 Brichau S., Respaut J.P. et Monié P.: New age constraints on emplacement of the Cévenol granitoids,
523 South French Massif Central, *Int J Earth Sci* 97:725–738, doi: 10.1007/s00531-007-0187-x, 2007.

524 Bruxelles L.: Dépôts et altérites des plateaux du Larzac central : causes de l’Hospitalet et de
525 Campestre (Aveyron, Gard, Hérault) Evolution morphogénétique, conséquences géologiques et
526 implications pour l’aménagement. Université d’Aix-Marseille I, Université de Provence, UFR
527 Sciences géographiques et de l’aménagement. Thèse, spécialité : Milieux physiques méditerranéens,
528 2001.

529 Calais, E., Freed, A. M., Van Arsdale, R., & Stein, S. (2010). Triggering of New Madrid seismicity by
530 late-Pleistocene erosion. *Nature*, 466(7306), 608–611. <http://doi.org/10.1038/nature09258>

531 Calais, E., T. Camelbeeck, S. Stein, M. Liu, and T. J. Craig (2016), A new paradigm for large
532 earthquakes in stable continental plate interiors, *Geophys. Res. Lett.*, 43, doi:10.1002/2016GL070815,
533 2016.

534 Calvet M., Gunnell Y., Braucher R., Hez G., Bourlès D., Guillou V., Delmas M. et ASTER team: Cave
535 levels as proxies for measuring post-orogenic uplift : Evidence from cosmogenic dating of alluvium-
536 filled caves in the French Pyrenees. *Geomorphology* 246 (2015) 617- 633 ; doi :
537 10.1016/j.geomorph.2015.07.013, 2015.

538 Camus H.: Vallée et réseaux karstiques de la bordure carbonatée sud-cévenole. Relation avec la
539 surrection, le volcanisme et les paléoclimats. Thèse de doctorat, Université Bordeaux 3, 692 p, 2003.

540 Champagnac J.D., Molnar P., Anderson R.S., Sue C. et Delacou B.: Quaternary erosion-induced
541 isostatic rebound in the western Alps. *Geology*, March 2007 ; v.35 ; no. 3 ; p. 195-198, doi : 10.1130/
542 G23053A.1, 2007.

543 Champagnac J-D. van der Beek P. Diraison G. et Dauphin S.: Flexural isostatic response of the Alps
544 to increased Quaternary erosion recorded by foreland basin remnants, SE France. *Terra Nova*, Vol 20,
545 No. 3, 213-220, doi : 10.1111/j.1365-3121.2008.00809.x, 2008.

546 Chéry J., Zoback M.D. et Hassani R.: An integrated mechanical model of the San Andreas Fault in
547 central and northern California. *J. Geophys. Res.*, 106(B10) :22051. 52,61, 2001.

548 Chéry, J., Genti, M. And Vernant, P. Ice cap melting and low-viscosity crustal root explain the narrow
549 geodetic uplift of the Western Alps. *Geophys. Res. Lett.* 43,1–8 (2016).

550 Child D.P., Elliott G., Mifsud C., Smith A.M and Fink D., Sample processing for earth science studies
551 at ANTARES. *Nuclear Instruments and Methods in Physics Research Section B Beam Interactions*
552 *with Materials and Atoms* 172(1-4):856-860 doi: 10.1016/S0168-583X(00)00198-1, 2000.

553 Corbel J.: Les phénomènes karstiques dans les Grands Causses. In : *Revue de géographie de Lyon*,
554 vol. 29, n°4, pp. 287-315, doi : 10.3406/geoca.1954.1990, 1954.

555 Dautria J.M., Liotard J.M., Bosch D., Alard O.: 160 Ma of sporadic basaltic activity on the Languedoc
556 volcanic line (Southern France): A peculiar cas of lithosphere-asthenosphere interplay. *Lithos* 120
557 (2010) 202-222, doi: 10.1016/j.lithos.2010.04.009, 2010

558 Genti M.: Impact des processus de surface sur la déformation actuelle des Pyrénées et des Alpes.
559 *Géophysique [physics.geo-ph]*. Université de Montpellier, 2015. Français. Thèse, 2016.

560 Granet M., Wilson M. et Achauer U.: Imaging a mantle plume beneath the French Massif Central.
561 Earth and Planetary Science Letters 136 (1995) 281-296, 1995.

562 Granger, D. E., Fabel, D. and Palmer, A.N.: Pliocene-Pleistocene incision of the Green River,
563 Kentucky determined from radioactive decay of comogenic ²⁶Al and ¹⁰Be in Mammoth Cave
564 sediments. *GSA Bulletin*; July 2001; v. 113; no. 7; p. 825–836

565 Granger, D. E., Kirchner, J. W., and Finkel, R. C.: Quaternary downcutting rate of the New River,
566 Virginia, measured from differential decay of cosmogenic ²⁶Al and ¹⁰Be in cave-deposited alluvium.
567 *Geology*; February 1997 ; v. 25 ; no.2 ; p. 107-110, 1997.

568 Granger D.E., Gibbon R.J., Kuman K., Clarke R.J., Bruxelles L. and Caffee M.W.: New cosmogenic
569 burial ages for Sterkfontein Member 2 Australopithecus and Member 5 Oldowan, *Nature Letter* 2015,
570 doi: 10.1038/nature14268, 2015.

571 Granger D.E. and Muzikar P.F.: Dating sediment burial with in situ-produced cosmogenic nuclides:
572 theory, techniques, and limitations. *Earth and Planetary Science Letters* 188 (2001) 269-281, 2001.

573 Granger D.E. and Stock G.M.: Using cave deposits as geologic tiltmeters : Application to postglacial
574 rebound of the Sierra Nevada, California. *Geophysical Research Letters*, vol. 31, L22501, doi :
575 10.1029/2004GL021403, 2004.

576 Zupan Hajna N., Mihevc A., Pruner P. and Bosák P. 2010. Palaeomagnetic research on karst sediments
577 in Slovenia. *International Journal of Speleology*, 39(2), 47-60. Bologna (Italy). ISSN 0392-6672,
578 2010.

579 Haq B.U., Herdenbol J. and Vail P.R.: Mesozoic and cenozoic chronostratigraphy and cycles of sea-
580 level change. *Society Economic Paleontologists Mineralogists Special Publication*, 42, 71-108, Tulsa,
581 Oklahoma. 1988.

582 Harmand D., Adamson K., Rixhon G., Jaillet S., Losson B., Devos A., Hez G., Calvet M. and Audra
583 P.: Relationships between fluvial evolution and karstification related to climatic, tectonic and eustatic
584 forcing in temperate regions, *Quaternary Science Reviews* (2017) 1-19, doi :
585 10.1016/j.quascirev.2017.02.016, 2017.

586 Hassani R. and Chery J., Anelasticity explains topography associated with Basin and Range normal
587 faulting. *Geology* 24(12):1095. doi: 10.1130/0091-7613(1996)024<1095:AETAWB>2.3.CO;2. 1996.

588 Hill C.A., 1999.. Sedimentology and Paleomagnetism of sediments, Kartchner caverns, Arizona.
589 *Journal of Cave and Karst Studies* 61(2) : 79-83, 1999.

590 Husson E.: Intéraction géodynamique/karstification et modélisation 3D des massifs carbonatés :
591 Implication sur la distribution prévisionnelle de la karstification. Exemple des paléokarsts créacés à
592 néogènes du Languedoc montpelliérain. *Sciences de la Terre. Université Montpellier 2- Sciences et*
593 *techniques du Languedoc*, 236 p, 2014.

594 Karst3D (2019). Karst3D data base. [https://doi.org/10.15148/940c2882-49f1-49db-a97e-](https://doi.org/10.15148/940c2882-49f1-49db-a97e-12303cace752)
595 [12303cace752](https://doi.org/10.15148/940c2882-49f1-49db-a97e-12303cace752)

596 Kooi H., Cloetingh S. et Burrus J.: Lithospheric Necking and Regional Isostasy at Extensional Basins
597 1. Subsidence and Gravity Modeling With an Application to the Gulf of Lions Margin (SE France),
598 *Journal of Geophysical Research* , vol. 97, no. B12, Pages 17,553- 17,571, november 10, 1992.

599 Leroux E., Rabineau M., Aslanian D., Granjeon D., Droz L. et Gorini C.: Stratigraphic simulations of
600 the shelf of the Gulf of Lions: testing subsidence rates and sea-level curves during the Pliocene and
601 Quaternary. *Terra Nova*, Vol 26, No. 3, 230-238, doi: 10.1111/ter.12091, 2014.

602 Lofi J., Rabineau M., Gorini C., Berne S., Clauzon G., De Clarens P., Dos Reis A.T., Mountain G.S.,
603 Ryan W.B.F, Steckler M.S. et Fouchet C.: Plio-Quaternary prograding clinoform wedges of the
604 western Gulf of Lion continental margin (NW Mediterranean) after the Messinian Salinity Crisis.,
605 *Marine Geology* July 2003; 198 (3-4) : 289-317, doi: 10.1016/S0025-3227(03)00120-8, 2003.

606 Lucazeau F. and Vasseur G.: Heat flow density data from France and surrounding margins, In: V.
607 Cermak, L. Rybach and E.R. Decker (Editors), *Tectonophysics*, 164 (1989) 251-258

608 Manchuel K., Traversa P., Baumont D., Cara M., Nayman E. Et Durouchoux C.: The French seismic
609 CATalogue (FCAT-17), *Bull Earthquake Eng* (2018) 16:2227–2251, doi: 10.1007/s10518-017-0236-1,
610 2018.

611 Miallier D., Michon L., Evin J., Pilleyre T., Sanzelle S., et Vernet G.: Volcans de la Chaîne des Puys
612 (Massif Central, France) : point sur la chronologie Vasset-Kilian-Pariou-Chopine. *Comptes Rendus*
613 *Géoscience*, Elsevier

614 Michon L. et Merle O.: The evolution of the Massif Central rift: Spatio-temporal distribution of the
615 volcanism. *Bulletin de la Society Geologique de France*, 2001, t. 172, n°2, pp. 201-211, doi:
616 10.2113/172.2.201, 2001.

617 Miller, K.G., Kominz, M.A., Browning, J.V., Wright, J.D., Mountain, G.S., Katz, M.E., Sugarman,
618 P.J., Cramer, B.S., Christie-Blick, N., Pekar, S.F.: The Phanerozoic record of global sea-level change.
619 *Science* 310, 1293–1298, doi : 10.1126/science.1116412, 2005.

620 Mocochain L.: Les manifestations géodynamiques –Externes et internes- de la crise de salinité
621 messinienne sur une plate-forme carbonatée peri-méditerranéenne : le karst de la basse ardèche
622 (moyenne vallée du Rhône ; France). Thèse de doctorat, Université Aix- Marseille I – Université de
623 Provence U.F.R des Sciences géographiques et de l'aménagement Centre Européen de Recherches et
624 d'Enseignement en Géosciences de l'Environnement., 196 p, 2007.

625 Molliex S., Rabineau M., Leroux E., Bourlès D.L., Authemayou C., Aslanian D., Chauvet F., Civet F.
626 et Jouët G.: Multi-approach quantification of denudation rates in the Gulf of Lion source-to-sink
627 system (SE-France). *Earth and Planetary Science Letters* 444 (2016) 101-115, doi :
628 10.1016/j.epsl.2016.03.043, 2016.

629 Nehlig P., Boivin P., de Goër A., Mergoïl J., Prouteau G., Sustrac G. Et Thiéblemont D.: Les volcans
630 du Massif central. *Revue BRGM: Géologues*, Numéro Spécial: Massif central, 2003.

631 Nguyen H. N., Vernant P., Mazzotti S., Khazaradze G. et Asensio E.: 3-D GPS velocity field and its
632 implications on the present-day post-orogenic deformation of the Western Alps and Pyrenees. *Solid*
633 *Earth*, 7 ; 1349-1363, 2016, doi : 10.5194/se-7-1349-2016, 2016.

634 Nocquet J.-M. et Calais E.: Crustal velocity field of western Europe from permanent GPS array
635 solutions, 1996-2001. *Geophys. J. Int.* (2003) 154, 72-88, doi : 10.1046/j.1365-246X.2003.01935.x,
636 2003.

637 Nocquet J.-M., Sue C., Walpersdorf A., Tran T., Lenôtre N., Vernant P., Cushing M., Jouanne F.,
638 Masson F., Baize S., Chéry J. and Van der Beek P.A., Present-day uplift of the western Alps, *Sci. Rep.*
639 6, 28404; doi: 10.1038/srep28404 (2016).

640 Olivetti V., Godard V., Bellier O. et ASTER team : Cenozoic rejuvenation events of Massif Central
641 topography (France) : Insights from cosmogenic denudation rates and river profiles. *Earth and*
642 *Planetary Science Letters* 444 (2016) 179-191, doi : 10.1016/j.epsl.2016.03.049 0012-821X, 2016.

643 Ouimet, WB, Whipple, KX, Crosby, BT, Johnson, JP, Schildgen, TF. 2008. Epigenetic gorges in
644 fluvial landscapes. *Earth Surface Processes and Landforms* **33**: 1993– 2009. doi: 10.1002/esp.1650
645 Epigenetic. 2008.

646 Rolland Y., Petit C., Saillard M., Braucher R., Bourlès D., Darnault R. Cassol D. Et ASTER Team:
647 Inner gorges incision history: A proxy for deglaciation? Insights from Cosmic Ray Exposure dating
648 (¹⁰Be and ³⁶Cl) of river-polished surfaces (Tinée River, SW Alps, France). *Earth and Planetary*
649 *Science Letters*, Elsevier, 2017, 457, pp.271 - 281, doi : 10.1016/j.epsl.2016.10.007. <hal-01420882>,
650 2017.

651 Rovey II C.W., Balco G., Forir M. Et Kean W.F.: Stratigraphy, paleomagnetism, and cosmogenic-
652 isotope burial ages of fossil-bearing strata within Riverbluff Cave, Greene County, Missouri.
653 *Quaternary Research* (2017), 1-13, doi : 10.1017/qua.2017.14, 2017.

654 Saillard M., Petit C., Rolland Y., Braucher R., BOurlès D.L., Zerathe S., Revel M. Et Jourdon A.: Late
655 Quaternary incision rates in the Vesubie catchment area (Southern French Alps) from in situ-produced
656 ³⁶Cl cosmogenic nuclide dating: Tectonic and climatic implications, *J. Geophys. Res. Earth Surf.*, 119,
657 1121–1135, doi:10.1002/ 2013JF002985. 2014.

658 Sanchis E. et Séranne M.: Structural style and tectonic evolution of a polyphase extensional basin of
659 the Gulf of Lion passive margin : the Tertiary Alès basin, southern France. *Tectonophysics* 322 (2000)
660 219-242, doi : 10.1016/S0040-1951(00)00097-4, 2000.

661 Sartégou A.: Évolution morphogénique des Pyrénées orientales: apports des datations de systèmes
662 karstiques étagés par les nucléides cosmogéniques et la RPE. *Géomorphologie*. Thèse de l'Université
663 de Perpignan. Français <NNT : 2017PERP0044>. <tel-01708921> , 2017.

664 Sartégou, A., Bourlès, D. L., Blard, P.-H., Braucher, R., Tibari, B., Zimmermann, L., et al. (2018a).
665 Deciphering landscape evolution with karstic networks_ A Pyrenean case study. *Quaternary*
666 *Geochronology*, 43, 12–29. <http://doi.org/10.1016/j.quageo.2017.09.005>

667 Sartégou A., Mialon A., Thomas S., Giordani A., Lacour Q., Jacquet A., André D., Calmels L.,
668 Bourlès D.L., Bruxelles L., Braucher R., Leanni L. Et ASTER team.: When TCN meet high school
669 students: deciphering western Cévennes landscape evolution (Lozère, France) sin g TCN on karstic
670 networks. Poster 4th Nordic Workshop on Cosmogenic Nuclides. 2018b.

671 Schaller M., von Blanckenburg F., Hovius N. Et Kubik P.W.: Large-scale erosion rates from in situ-
672 produced cosmogenic nuclides in European river sediments. *Earth and Planetary Science Letters* 188
673 (2001) 441-458, 2001.

674 Séranne M., Benedicto A., Labaum P., Truffert C. et Pascal G.: Structural style and evolution of the
675 Gulf of Lion Oligo-Miocene rifting : role of the Pyrenean orogeny. *Marine and Petroleum Geology*,
676 Vol. 12, No. 8, pp. 809-820, 1995.

677 Séranne M., Camus H., Lucazeau F., Barbarand J. et Quinif Y.: Surrection et érosion polyphasées de la
678 Bordure cévenole. Un exemple de morphogenèse lente. *Bull. Soc. Géol. France*, 2002, t. 173, n°2, pp.
679 97-112, 2002.

680 Sibuet J.-C., Srivastava S.P. et Spakman W.: Pyrenean orogeny and plate kinematics. *Journal of*
681 *Geophysical Research: Solid Earth*, Vol 109, doi: 10.1029/2003JB002514 , 2004.

682 Spassov S. et Valet J.-P.: Detrital magnetisations from redeposition experiments of different natural
683 sediments. *Earth and Planetary Science Letters* 351-352 (2012) 147-157, doi:
684 10.1016/j.epsl.2012.07.016, 2012

685 Stewart J. and Watts A.B.: Gravity anomalies and spatial variation of flexural rigidity at mountain
686 ranges. *Journal of Geophysical research*, vol 102, no. B3, Pages 5327-5352, march 10, 1997, doi:
687 10.1029/96JB03664, 1997.

688 Stock G.M., Granger D.E., Sasowsky I.D., Anderson R.S. et Finkel R.C.: Comparison of U-Th,
689 paleomagnetism, and cosmogenic burial methods for dating caves : Implications for landscape
690 evolution studies. *Earth and Planetary Science Letters* 236 (2005) 388-403, doi :
691 10.1016/j.epsl.2005.04.024, 2005.

692 Tarayoun A., Mazzotti S., Gueydan F., Quantitative impact of structural inheritance on present-day
693 deformation and seismicity concentration in intraplate deformation zones, *Earth and Planetary*
694 *Science Letters*, Volume 518, 2019, Pages 160-171, ISSN 0012-821X, doi:
695 10.1016/j.epsl.2019.04.043., 2017.

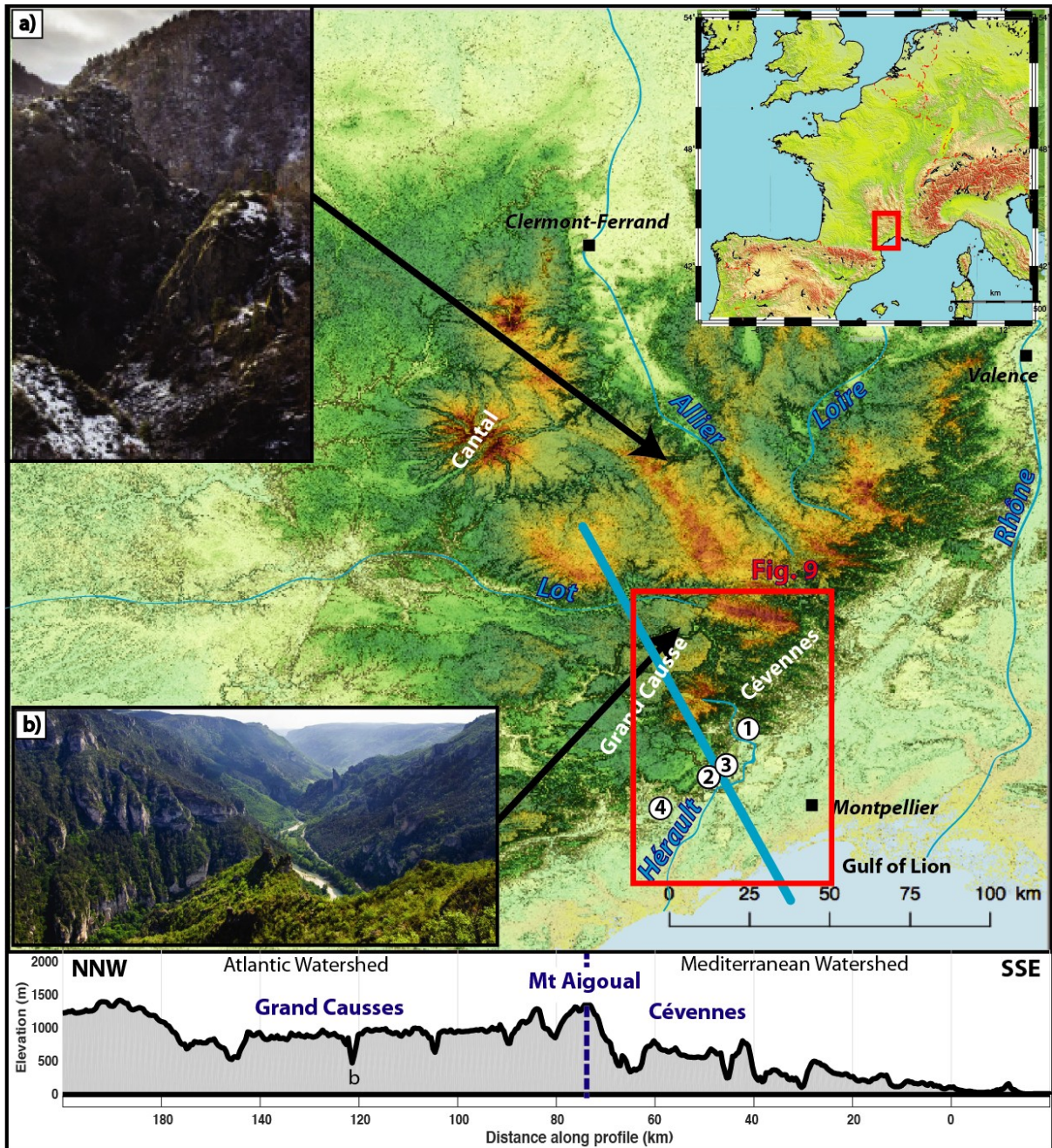
696 Tassy A., Mocochain L., Bellier O., Braucher R., Gattacceca J., Bourlès D.: Coupling cosmogenic
697 dating and magnetostratigraphy to constrain the chronological evolution of peri-Mediterranean karsts
698 during the Messinian and the Pliocene: Example of Ardèche Valley, Southern France. *Geomorphology*,
699 189 (2013), pp. 81-92, doi: 10.1016/j.geomorph.2013.01.019, 2013.

700 Tauxe L., Steindorf J.L. et Harris A.: Depositional remanent magnetisation: Toward an improved
701 theoretical and experimental foundation. *Earth and Planetary Science Letters* 244 (2006) 515-529, doi:
702 10.1016/J.epsl.2006.02.003, 2006.

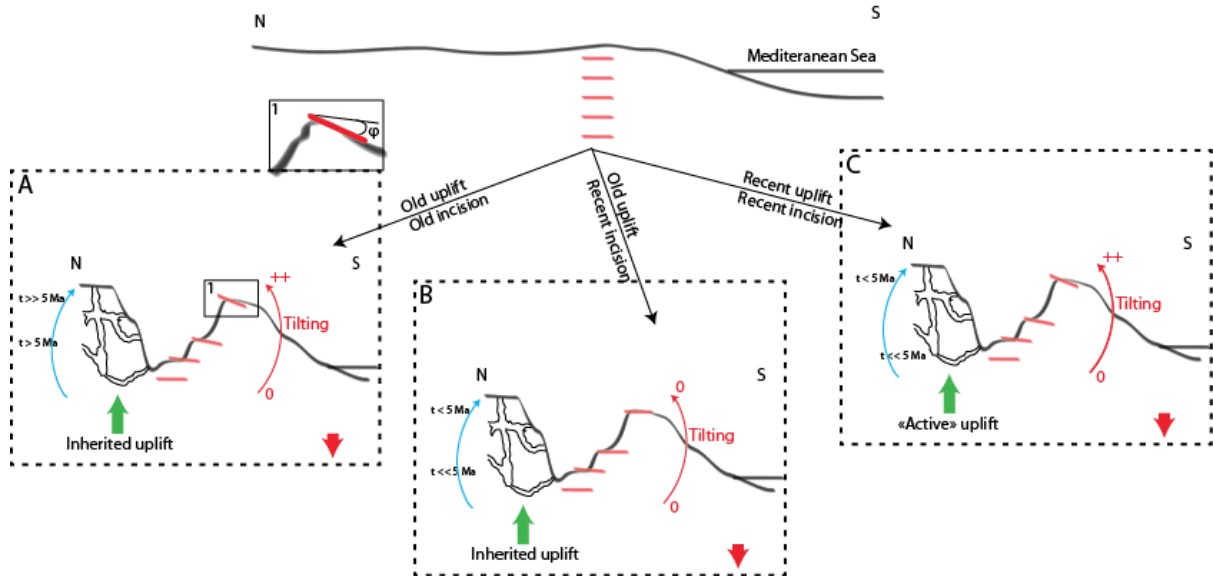
703 Tricart P. : From passive margin to continental collision: A tectonic scenario for the western Alps.
704 *American journal of science*, Vol. 284, February, 1984, P97-120, 1984.

705 Vernant, P., Hivert, F., Chéry, J., Steer, P., Cattin, R., & Rigo, A. (2013). Erosion-induced isostatic
706 rebound triggers extension in low convergent mountain ranges. *Geology*, 41(4), 467–470.
707 <http://doi.org/10.1130/G33942.1>

708



709
 710 **Figure 1: 30 m resolution DEM of the French Massif-Central with slope shading. Examples of finite**
 711 **incision typical of the French Massif-Central in a) crystalline area (Seuge Canyon) and b) limestone**
 712 **plateau (Tarn Canyon) The red box shows the Location of the study area and fig. 9. Numbers**
 713 **indicate sampling sites; TCN measurements: 1) Rieutord Canyon (43,958°N; 3.709°E);**
 714 **Paleomagnetic analysis: 2) Leicasse Cave System (43,819°N; 3.56°E) and 3) Garrel Cave system**
 715 **(43,835°N; 3.616°E); dated basaltic flows: 4) Lodève basin (43,669°N; 3.382°E). Bottom panel is an**
 716 **example of typical topographic profile used for numerical model set up, its location is given by the**
 717 **blue line on the map.**
 718 **Note the north-western area with large limestone plateaus dissected by canyons (Grands Causses),**
 719 **and the rugged crystalline area with steep valleys (Cévennes).**



720
721
722
723
724
725
726
727
728
729

Figure 2: conceptual models for landscape evolution. Top panel is the initial stage (prior to uplift). Each panel represent a possible scenario explaining current morphology: A) Old uplift and old incision, B) Old uplift and recent incision and C) both recent uplift and incision. Blue arrow and associated ages show expected result (or absence of) for burial dating. Red level represents fossilized morphological markers, cumulating (or not) the differential uplift by finite tilting.



730
731
732
733
734
735
736
737

Figure 3: Example of quartz cobbles sampled for burial dating. Location: Cuillère Cave

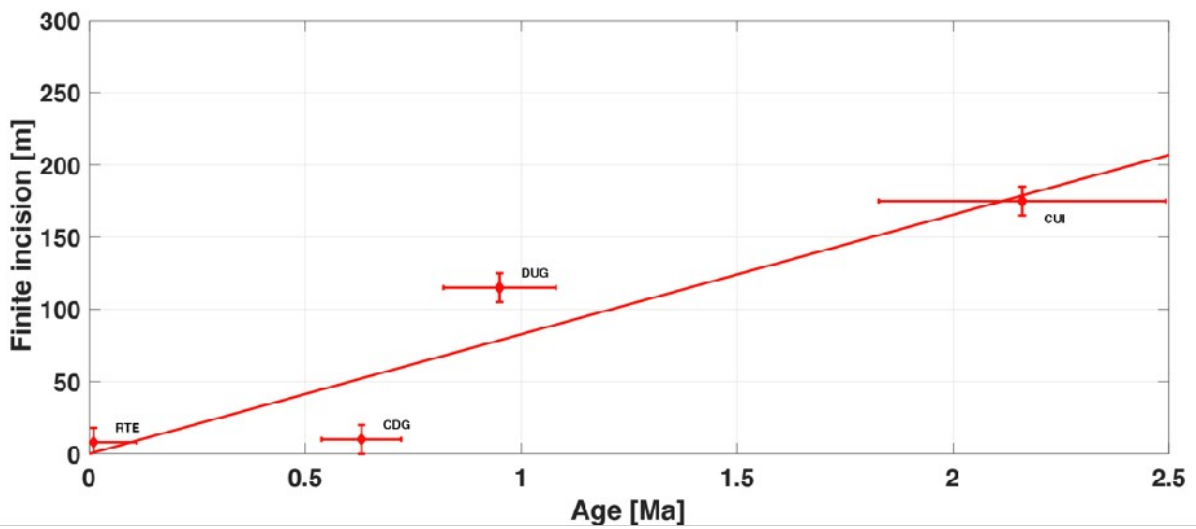


738

739 **Figure 4: Example of clay sampling for the paleomagnetic study. Location at the entrance shaft of the Le-**
 740 **icasse Cave system. With a ~580 m a.s.l. elevation, they are the highest samples.**

741

742



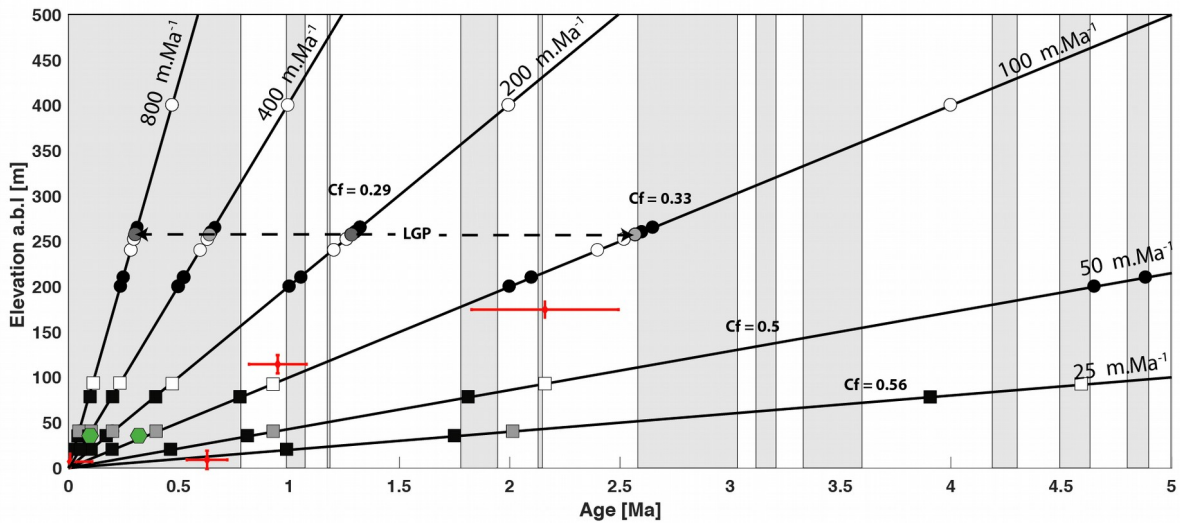
743

744 **Figure 5: Relation finite incision-burial age for the Rieutord canyon. Finite incision is the elevation**
 745 **of the sampling site relatively to the current riverbed. RTE for Route Cave, CDG for Camp de Guerre**
 746 **Cave, DUG for Dugou Cave and CUI for Cuillère Cave**

747

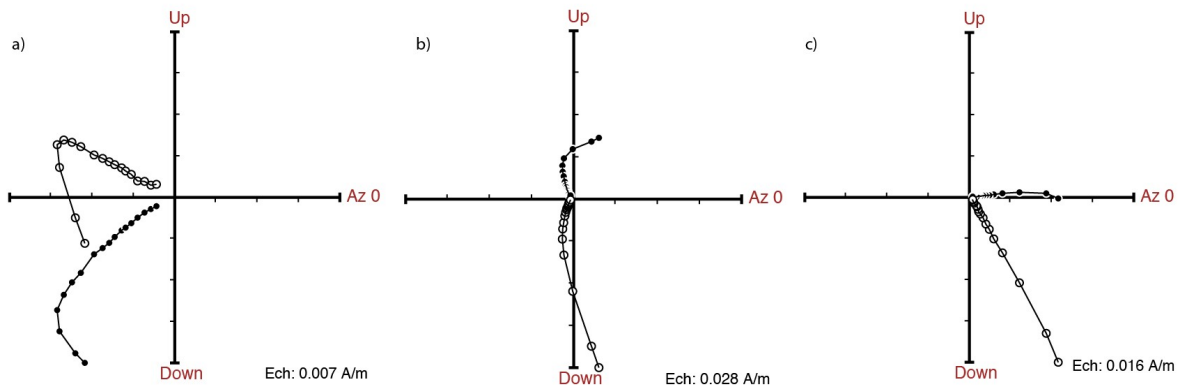
748

749



750
 751 **Figure 6. Constraining the incision rate in the Cevennes margin, using paleomagnetic polarities**
 752 **from clay deposits (black, grey and white symbols) and burial ages (red crosses): Circles are**
 753 **from the Leicasse cave with LGP being *les gours sur pattes* profile (see text), squares are from**
 754 **the Garrel cave. Black, grey and white symbols correspond to normal, transitional and reverse**
 755 **polarities, respectively. Black linear straight lines define possible incision rates that are sup-**
 756 **posed constant over the study time period. Cf values are the correlation factors between the**
 757 **measured paleomagnetic polarities and the predicted paleomagnetic scale (see also Figure 8).**
 758 **Green hexagons show the U/Th ages obtained in the Garrel by Camus (2003).**

759
 760



761
 762
 763
 764 **Figure 7: Zijderveld Diagram for three samples from the Gours-sur-Pattes (Leicasse) site.**
 765 **Stratigraphical order is from a) (the older, base of the profile) to c) (the younger, top of the**
 766 **profile.**

768 **Figure 8: Linear incision rate fit to the paleomagnetic data (blue) and TCN burial ages (red). The**
769 **blue curve is the normalized correlation between theoretical and observed polarities. The highest**
770 **correlation corresponds to the best incision rates. The red curve is the RMSE between the modeled**
771 **and the observed burial ages shown on Fig. 4, the lower the RMSE, the better the fit.**

772

773

774

775

776

777

778

779

780

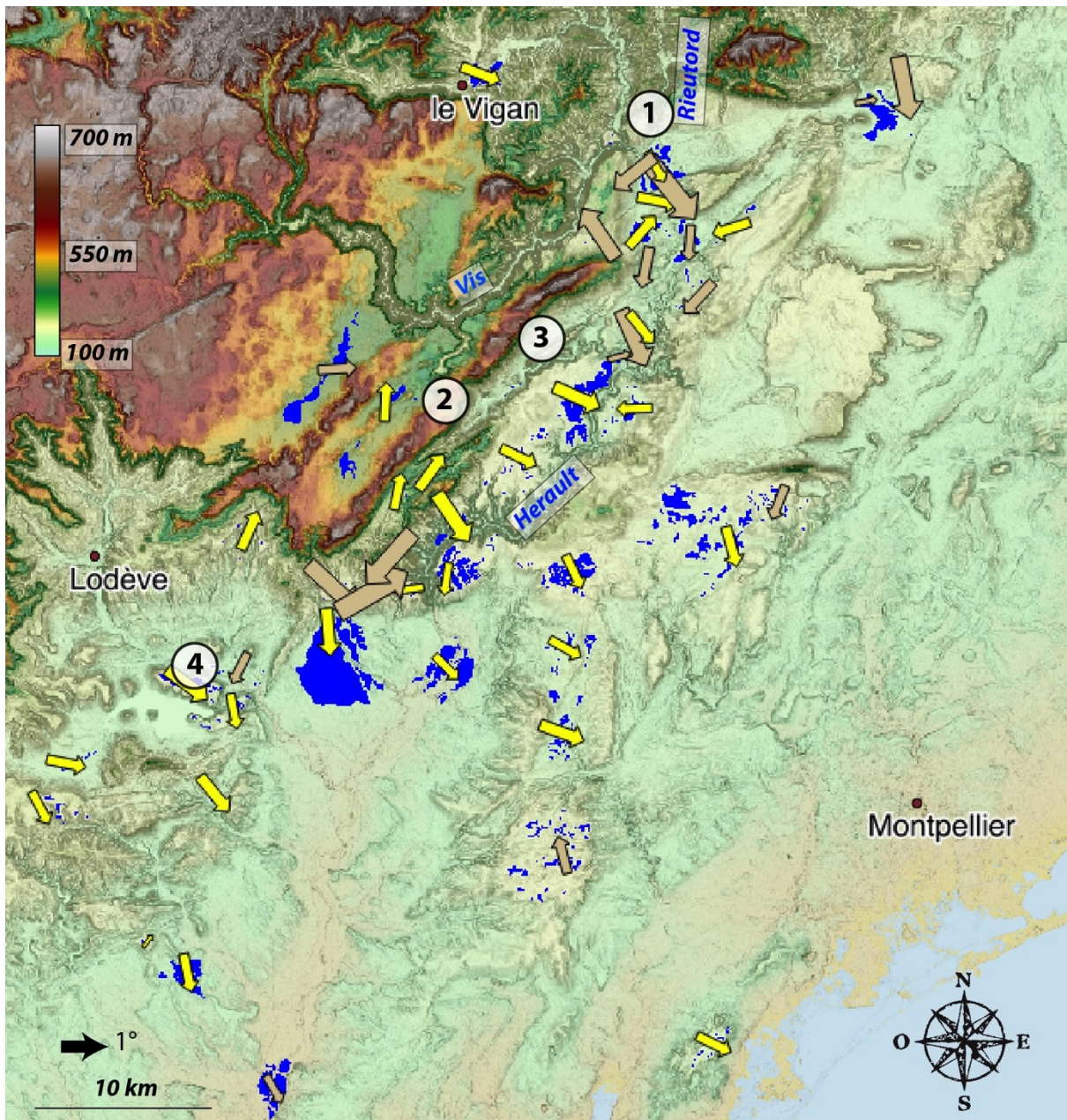
781

782

783

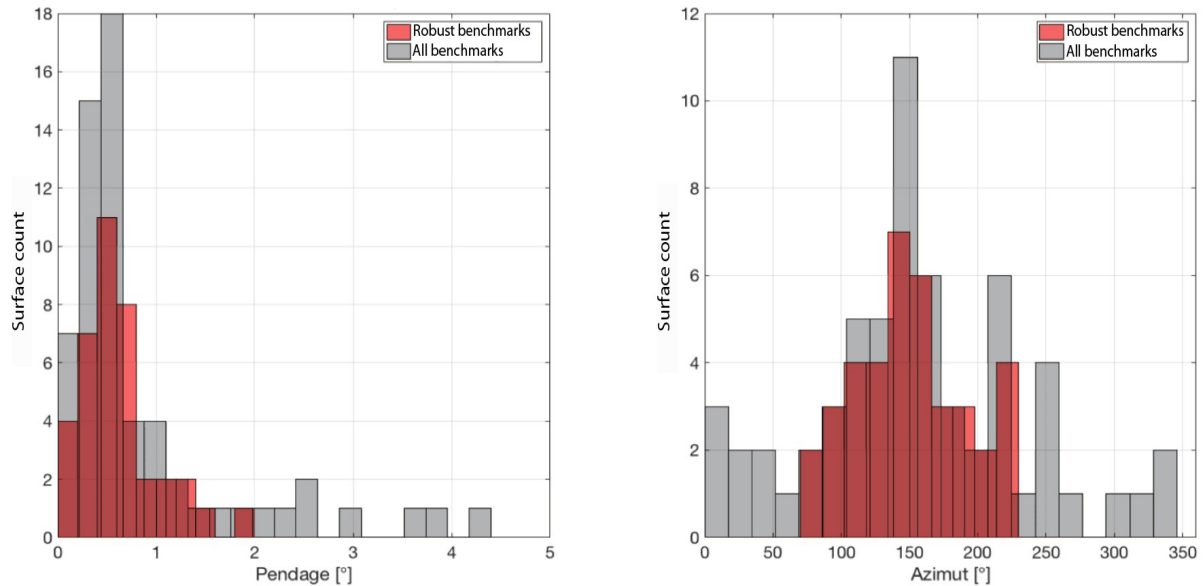
784

767



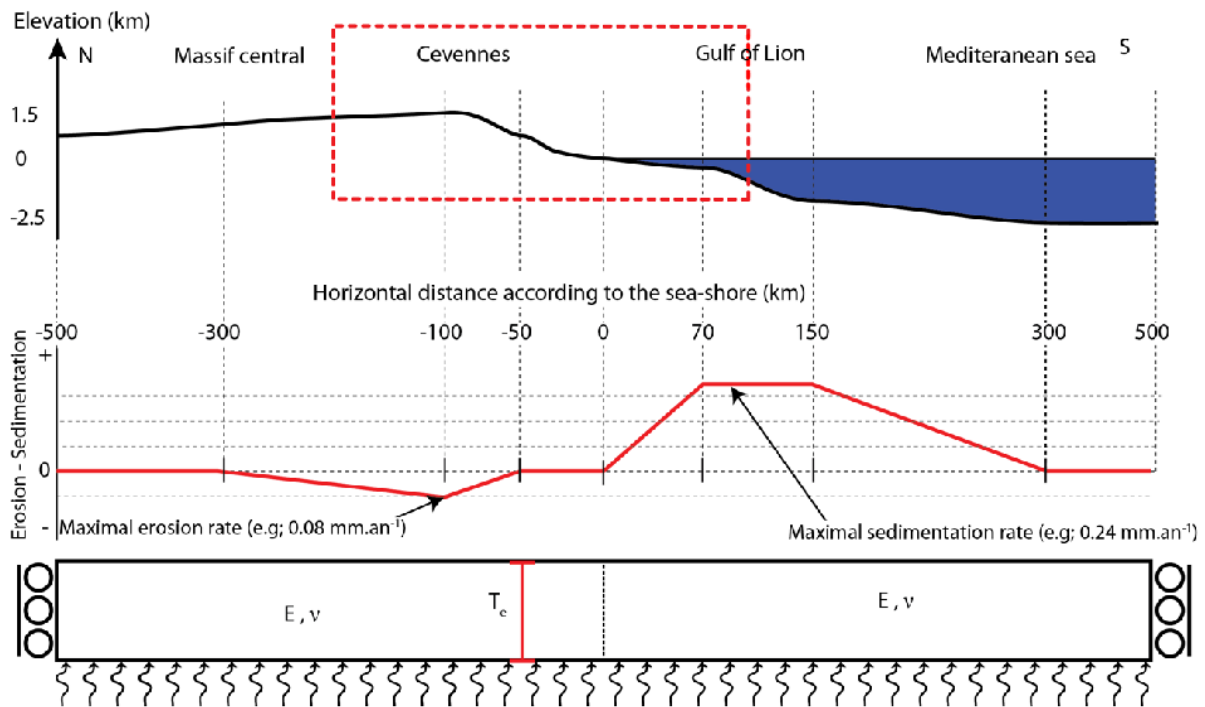
786
 787 **Figure 9: Color-coded-altitude map based on a 30 m resolution DEM with slope shading with tilted**
 788 **geomorphologic surfaces indicated by blue polygons. . The vectors show the marker dip direction**
 789 **and are proportional to the tilt angle (the larger vectors are for higher tilts). Yellow and brown**
 790 **vectors are for robust and rejected surfaces respectively. Several vectors are hidden due to their**
 791 **close proximity to the larger ones. Numbers indicate the sampling sites: 1) Rieutord Canyon, 2)**
 792 **Leicasse Cave System, 3 Garrel Cave system and 4) Lodève basin. See Fig. 1 for geographic**
 793 **coordinates.**

794
 795
 796
 797
 798



799 **Figure 10: Tilt and azimuth distribution.** Left panel is density distribution for surface maximum
 800 tilt in degree. Right panel is the dip azimuth relative to the north. For each histogram, red and grey
 801 populations are for robust and primary detected markers.
 802

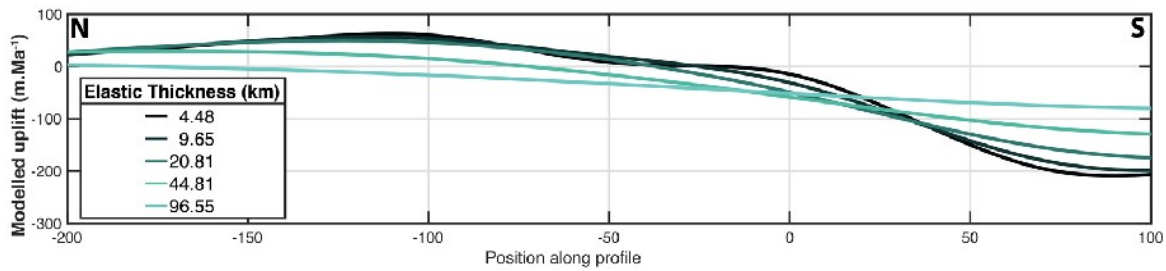
803
 804
 805



806
 807
 808 **Figure 11: Top panel: simplified topographic profile.** The red box corresponds to the area shown
 809 on figs. 1 and 9. Mid panel, surface processes profile, negative values are for erosion and positive
 810 values for sedimentation. Bottom panel: model set-up with two compartments (one for the
 811 Cevennes area and one for the gulf of lion). The base of the model is supported by hydrostatic
 812 pressure and the right and left boundaries are free to move vertically but their horizontal
 813 velocities are set to 0 mm/yr. T_e is the equivalent elastic thickness (in km), E (Pa) and ν are the
 814 Young modulus and the Poisson coefficient respectively whom values are independent in each
 815 compartment.
 816

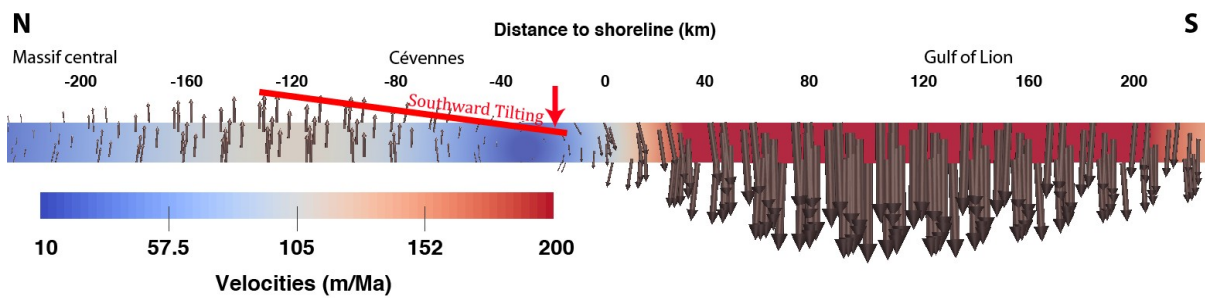
817

818



819

820 **Figure 12: Modelled uplift according to different elastic thickness (Te). Most probable Te are between**
 821 **10 and 30 km.**



822

823 **Figure 13: Modelling result for Te= 15km. Erosion-sedimentation rate profile is the same as in fig.**
 824 **9. The vectors show the velocity field and the intensity is given by the background color code.**
 825 **Black values on top are distance relative to the sea-shore (positive value offshore and negative**
 826 **values inland). The red line represents the southward modelled tilting due to differential uplift.**

827

Cave	Lat	Lon	Elevation	height (a.b.l.)	¹⁰ Be conc (atom/g)	σ ¹⁰ Be (atom/g)	²⁶ Al conc (atom/g)	σ ²⁶ Al (atom/g)	²⁶ Al/ ¹⁰ Be (and error)	Burial age (Ma)	Burial age error (Ma)
RTE	43,960	3,707	175	8	3,54E+04	1,18E+03	2,16E+05	1,47E+04	6,11 +/-0.46	0,20	+0.16/-0.15
CDG	43,955	3,710	185	10	8,87E+04	3,12E+03	4,29E+05	3,28E+04	4,83 +/-0.41	0,67	+0.18/-0.16
DUG	43,957	3,711	245	115	1,27E+04	5,68E+02	5,29E+04	6,36E+03	4,15 +/-0.53	0,99	+0.28/-0.25
CUI	43,959	3,711	354	175	1,70E+04	7,14E+02	3,75E+04	5,28E+03	2,20 +/-0.32	2,28	+0.33/-0.28

828

829 Table 1: Samples analytical results and parameters. Cave code are: RTE for the “de la route” Cave, CDG for the
 830 “Camp de Guerre” cave, DUG for the “Dugou” Cave and CUI for the “Cuillère” Cave. Main parameters are the
 831 geographical coordinate (Lat, Lon in decimals degree), the elevation (a.s.l), the height (a.b.l., computed
 832 relatively to the surface river elevation. The concentration (atoms/g quartz) of ¹⁰Be and ²⁶Al in collected sand
 833 samples are all AMS ¹⁰Be/Be and ²⁶Al/Al isotopic ratios corrected for full procedural chemistry blanks and
 834 normalized to KN-5-4 and KN -4-2, respectively. The error () is for total analytical error in final average ¹⁰Be
 835 and ²⁶Al concentrations based on statistical counting errors in final ¹⁰Be/Be (²⁶Al/Al) ratios measured by

836 AMS in quadrature with a 1% error in ^9Be spike concentration (or a 4% error in ^{27}Al assay in quartz) and a
837 2% (or 3%) reproducibility error based on repeat of AMS standards. Burial age (minimum) assuming no post-
838 burial production by muons at given depth (all deeper than 30m) in cave below surface and assuming initial
839 $^{26}\text{Al}/^{10}\text{Be}$ ratio is given by the production ratio of 6.75. The burial age error determined by using a $\pm 1\sigma$ range
840 in the measured $^{26}\text{Al}/^{10}\text{Be}$ ratio

841